13th International Symposium on Particle Image Velocimetry – ISPIV 2019
Munich, Germany, July 22-24, 2019

Velocity and pressure reconstruction from sparse particle fields

Karuna Agarwal[1], Omri Ram[1], Jin Wang[1], Joseph Katz[1]*

[1]Johns Hopkins University, Department of Mechanical Engineering, Baltimore, USA

*katz@jhu.edu

Abstract

This paper introduces the Constrained Cost Minimization (CCM) technique to interpolate unstructured sparse particle tracks and get velocity, velocity gradients, material acceleration, and hence pressure on Eulerian grids. The technique incorporates known information like the divergence-free condition of velocity and curl-free condition of material acceleration to improve the reliability of reconstruction of the flow, compensating for sparse data. The method is tested for sub-sampled simulations of a 2D double-gyre system, artificial tracks from DNS of turbulent channel flow, as well as tomographic experiments for a shear layer. The results show that even with sparse data, lower than comparable experimental limits, we achieve interpolation errors of <1%.

1 Introduction

Reliable pressure measurements are critical in understanding a variety of flows, for example, determining lift and drag forces on bodies, measuring the noise radiated from surfaces or understanding cavitation phenomena. Resolving pressure within vortices and pressure-strain correlations is significant to turbulence research. Recently introduced methods have been based on calculating the pressure from the time-resolved velocity field either by spatially integrating the material acceleration or solving the pressure-Poisson Equation (Van Oudheusden 2013). These calculations are mostly performed on a regularized grid.

While unstructured trajectories can also yield useful information- finite time Lyapunov exponents to get a measure of chaos or to find Lagrangian coherent structures; it is, however, still a challenge to get the pressure statistics from the tracks directly. Neeteson et. al 2015 have solved Pressure Poisson equations on unstructured grids formed by Delaunay triangulation and Voronoi tessellations but this requires dense particle distributions; $N^* > 1000$ where N^* is the number of particles in the characteristic volume.

There are two approaches for calculating the material acceleration from 3D particle tracks: (i) projecting the velocity onto regular grids using e.g. a Singular Value Decomposition (SVD) interpolation scheme (Talapatra et al. 2012), and then calculating the acceleration using a pseudo-Lagrangian (Liu and Katz 2013) or Eulerian approach, (ii) determining the material acceleration first and then interpolating it onto a regular grid (Schanz et al. 2016). This can also be implemented using the SVD scheme.

In the second order SVD implementation, the contribution of each measurement point in the interpolation volume is affected by its 3D location relative to the grid point, as well as the spatial gradients and curvature. Thus, the spatial gradients are obtained directly from the interpolation, eliminating the need for finite differencing. However, it requires at least 10 measurements within the interpolation volume to be feasible and 15-30 particles for high accuracy, restricting the spatial resolution in cases with sparse data.

There exist varied practical limitations on particle seeding density for Particle Tracking Velocimetry (PTV) such as low spatial resolution, 3D reconstruction errors, difficulty matching to nearest neighbors. To augment sparse data, Schneiders et al. (2016) introduce an iterative interpolation technique based on satisfying the vorticity transport equation. This vortex-in-cell (VIC) method uses radial basis functions of prescribed sizes to get the vorticity while ensuring the fitted velocity data linearly interpolates to measurements. Gesemann (2015) has proposed the FlowFit technique that fits the data using B-splines while penalizing high wave-numbers and the divergence of velocity. The resulting function is optimized using conjugate gradients for least squares.

2 Methods

We introduce an alternative approach based on Constrained Cost Minimization (CCM) of tapered weighted least squares (Wunsch 1996). A cost function J is defined as

$$J = (y - \boldsymbol{A}x_i)^T \boldsymbol{W}(y - \boldsymbol{A}x_i) + k(x_i - x_{i-1})^T \boldsymbol{S}(x_i - x_{i-1}) + 2\lambda\,(B^T x_i) \quad (1)$$

where x_i is the velocity or material acceleration vectors and its derivatives on each grid point. It is a 30×1 vector for second order mapping in 3D. Iteration number is denoted by the subscript i.

In the first term, y is a vector containing all the velocity/acceleration measurements in the interpolation volume, $\boldsymbol{A}$ the local tensor fit (mapping x_i into y) based on the Taylor's series expansion identical to SVD, and $\boldsymbol{W}$ is a weight tensor, chosen as the inverse of the variance in the measurements. $\boldsymbol{W}$ can also be ascribed weights based on known measurement errors, especially when less than 3 particles are present in the interpolation volume and therefore variance is not a good choice. Outliers can be assigned minimal weights or eliminated. $\boldsymbol{A}$ contains the information of the distance of the particle from grid point r, so has O(1), O(r), O(r^2) terms so care has to be taken to scale the physical dimensions such that $\boldsymbol{A}$ is well-conditioned. A scale factor proportional to the condition number of $\boldsymbol{A}$ is used. This is done for all the sparse SVD results presented here as well.

The second term accounts for deviations from prior estimates, starting from the SVD values (x_0). Here, $\boldsymbol{S}$ is a weight tensor defined as the inverse of the variance in x_0 in the interpolation volume. This is the taper or regularization that enables us to invert the problem; without which SVD would just yield an x_i with minimized norm. To ensure convergence of iterations, the allowed deviation from x_{i-1} needs to be controlled, which is done by varying the weight scale k. The scale is found to be such that we allow for larger deviation and the importance of the second term is lower than the first term, with $k = 0.1 - 0.01$. Only the order of magnitude of the constant is significant, and it is the same for a given experiment irrespective of the seeding density or the noise. Figure 1 illustrates how k is selected for the case of synthetic tracks from DNS of a turbulent channel flow.

The third term introduces a physical constraint, e.g. $\nabla \cdot u = 0$ for the velocity or $\nabla \times \frac{Du}{Dt} = 0$ for the acceleration, using a Lagrange multiplier λ. This multiplier is a measure of sensitivity to the constraints.

Imposing $\partial J/\partial x_i$ =0 and $B^T x_i = 0$, one obtains a closed-form solution for x_i and λ using the singular values (Moore-Penrose inverse) of $(\boldsymbol{A}^T\boldsymbol{W}\boldsymbol{A} + k\boldsymbol{S})$. The results converge in 2-4 iterations. This analysis is performed over a volume set to contain 4-6 particles while the initial SVD volume is set to contain 12-15 particles. For a grid size of 50×30×20, the procedure takes 20-30s to run using MATLAB on a standard PC. It is can be parallelized since each grid point calculation is independent of others. Once the material acceleration is interpolated, we spatially integrate using a GPU-based parallel-line, omni-directional technique (Wang et. al. 2019).

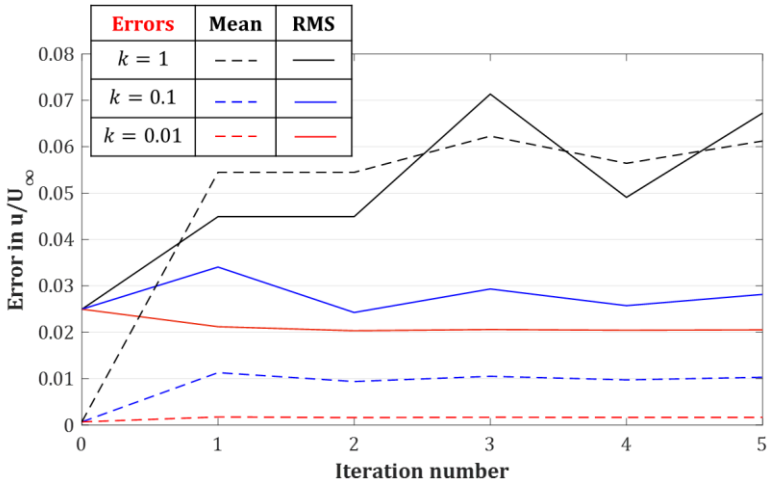

Figure 1: Mean and rms errors in velocity for synthetic boundary layer simulations with iterations i.

3 Results

The CCM interpolation method is validated for sparsely seeded simulation of an oscillating double-gyre system (Shadden et al. 2005) and DNS of turbulent channel flow (Graham et al. 2016). It is also applied to tomographic PTV data for a turbulent shear layer in the region most prone to cavitation inception.

3.1 Double gyre system

A double gyre system with the stream function defined as: $\psi = Asin(\pi y)\sin(\pi(x^2\epsilon sin\omega t + x - 2x\epsilon sin\omega t)$. A is chosen as 0.1 to make the peak velocity in each direction as 0.1π, the frequency of oscillation is set as 1 by choosing $\omega = 2\pi$, the amplitude of the oscillation $\epsilon = 0.25$. Figure 2(a) shows the original velocity, Figure 2(b) shows the SVD results based on 45 randomly scattered particles ($N^* = 22.5$), and Figure 2(c) shows the corresponding CCM results. CCM captures the size and location of the core of the vortex. Figure 3 shows the errors in acceleration vectors and the curl of acceleration for the two methods. The errors in acceleration for CCM is diminished while the curl disappears. Table 1 lists the errors in velocity, vorticity and material acceleration scaled by the peak values in the prescribed field for both the SVD and CCM techniques at different seeding densities. Consistently CCM reduces errors compared to the SVD method.

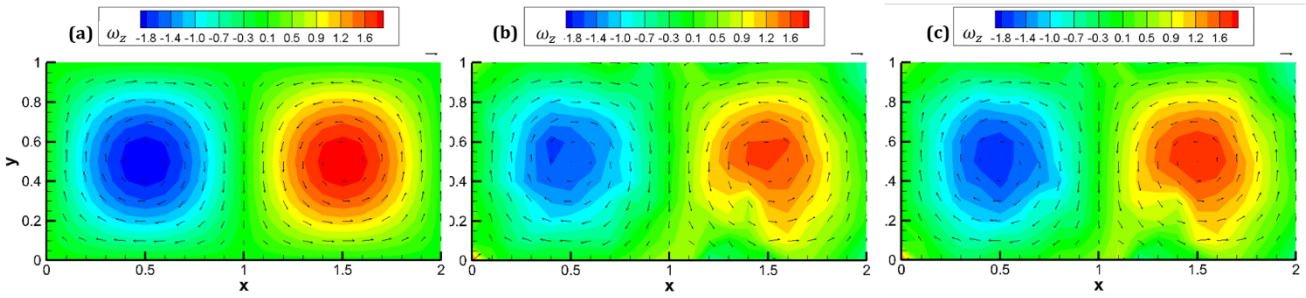

Figure 2: Velocity vectors and vorticity contours of the 2D gyre: (a) original field, (b) results of SVD interpolation based on a total of 45 synthetic particle traces, and (c) results of CCM analysis initiated using the SVD data.

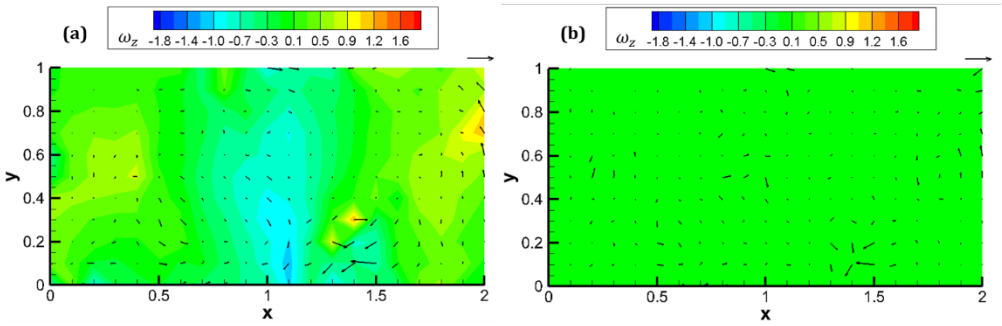

Figure 3: Acceleration error vectors and vorticity contours of the 2D gyre: (a) results of SVD interpolation based on a total of 45 synthetic particle traces, and (b) results of CCM analysis initiated using the SVD data. Reference vector of length 0.3 is shown.

Table 1. Scaled errors (mean±rms) for the two interpolation methods for various seeding densities

Particle seeding	Error in velocity		Error in vorticity		Error in acceleration	
N^*	SVD	CCM	SVD	CCM	SVD	CCM
10	0.07±0.32	0.06±0.23	0.014±0.25	0.015±0.22	0.051±0.33	0.047±0.29
22.5	0.015±0.092	0.014±0.068	0.02±0.13	0.006±0.11	0.032±0.17	0.025±0.15
50	0.005±0.036	0.002±0.031	0.003±0.081	0.002±0.077	0.009±0.075	0.004±0.046
100	0.003±0.026	0.002±0.018	0.005±0.051	0.005±0.048	0.001±0.04	0.001±0.05
500	0.00±0.002	0.00±0.0014	0.00±0.009	0.00±0.008	0±0.0034	0.00±0.0023

3.2 Turbulent boundary layer

For the turbulent boundary layer, synthetic tracks are obtained using DNS data for channel flow with $Re_\tau = 1000$. The volume, 125×75×47.5 in wall units, contains 2500 randomly distributed particles. The grid size is 2.5 wall units and based on DNS grid size N^*= 0.004. The rms of errors in velocity are plotted in Figure 4 and material acceleration in Figure 5. Results before and after adding 1% and 5% noise are shown. While the added noise increases the error, CCM systematically reduces these errors. The errors are comparable to dense data interpolation presented in Wang et. al. 2018.

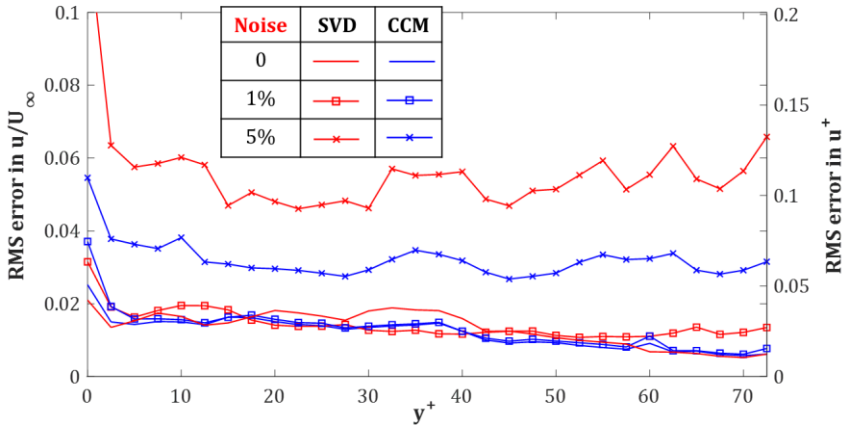

Figure 4: Comparison of errors in velocity interpolation from 2500 particles in a turbulent channel flow. All the SVD results are in red and CCM results in blue.

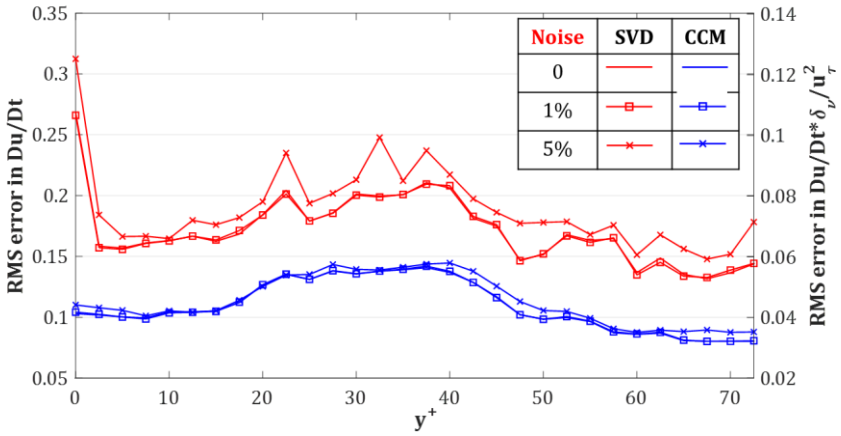

Figure 5: Comparison of errors in material acceleration interpolation from 2500 particles in a turbulent channel flow. All the SVD results are in red and CCM results in blue.

3.2 Turbulent shear layer

For a shear layer, cavitation incepts in secondary vortices. Experiments using backward facing step was performed to study this phenomenon. More details of the setup can be found in Agarwal et. al. 2018. To relate the pressure field to the behavior of the cavities, time-resolved volumetric PTV is performed. The "Shake-the-Box" method is used for processing Tomographic PIV data to get the unstructured velocity and material acceleration in the 12.5×7.5×4 mm volume. The vector spacing needed to well-resolve the secondary vortices which are 1-2 mm in diameter and 5-7 mm in length is 250 µm, corresponding to 12-18 voxels. A total of 3000-4000 tracks are resolved, giving us $N^* = 150 - 200$.

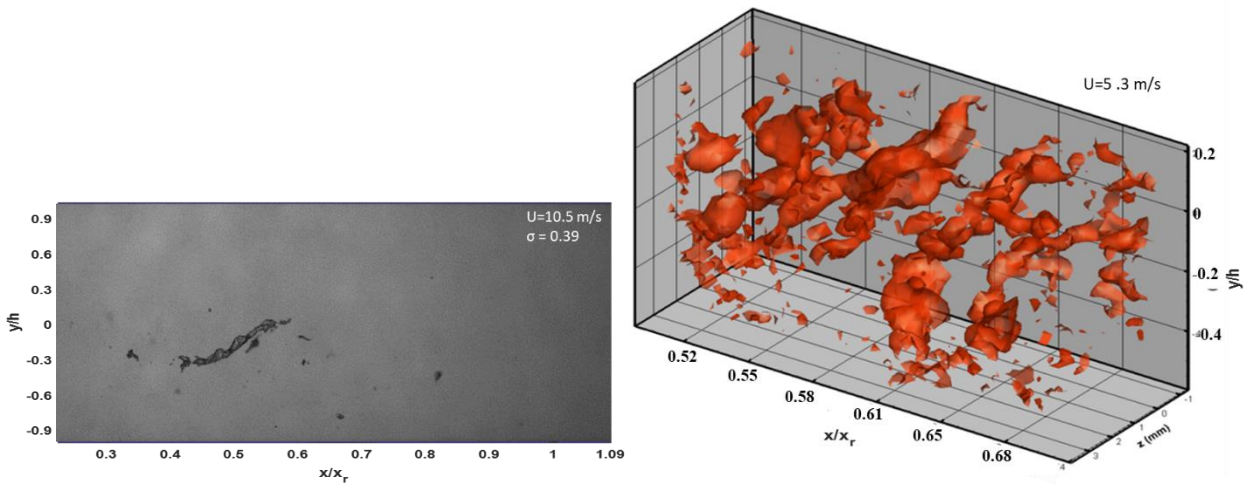

Figure 6: Samples of instantaneous: (a) image showing cavitation in a quasi-streamwise vortex; (b) iso-surfaces of λ_2 obtained using tomographic PIV (STB), and interpolated using CCM.

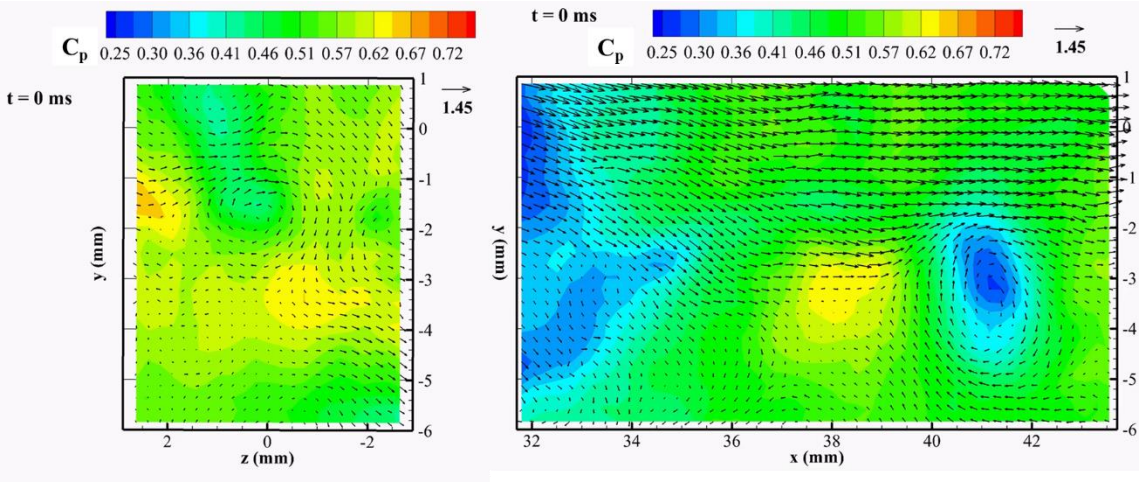

Figure 7. Instantaneous coefficients of pressure along with the velocity vectors in the central (a) yz plane and (b) xy plane.

A sample visualization of the cavitation in streamwise vortices and an instance of dominant coherent structures (λ_2 = -350000 1/s^2) showing quasi-streamwise vortices is presented in Figure 6. These structures appear intermittently, and persist for periods of 2-5 ms, consistent with the observed duration of cavitation events. Figure 7 shows $C_p = (P - P_{ref})/0.5\rho U^2$ where P is the pressure obtained by integration of the interpolated material acceleration, P_{ref} is the reference pressure, ρ the density of water and U is the freestream velocity of 1.45 m/s. High pressure regions are associated with saddle-points of the velocity distribution and low-pressure associated with the vorticity.

4 Conclusions

The CCM technique for interpolation of velocity and material acceleration from sparse particle tracks is introduced. It is a tapered weighted least squares formulation constrained using Lagrange multipliers that leverages the mass and momentum conservation laws to reduce the interpolation errors. We tested for synthetic data for an oscillating gyre system as well as DNS of channel flow. The errors diminish with particle density and lesser experimental noise but CCM is able to more effectively suppress noise. This technique is now being implemented to understand the scaling of pressure in the secondary vortices where cavitation incepts in a shear layer.

Acknowledgements

This project is supported by ONR MURI grant: Predicting Turbulent Multi-Phase Flows with High Fidelity - A Physics-Based Approach.

References

Van Oudheusden, B. W. (2013) PIV-based pressure measurement. Measurement Science and Technology 24(3): 032001.

Talapatra, S., & Katz, J. (2012) Three-dimensional velocity measurements in a roughness sublayer using microscopic digital in-line holography and optical index matching. Measurement Science and Technology 24(2): 024004.

Liu, X., & Katz, J. (2013) Vortex-corner interactions in a cavity shear layer elucidated by time-resolved measurements of the pressure field. Journal of Fluid Mechanics 728: 417-457.

Schanz, D., Gesemann, S., & Schröder, A. (2016) Shake-The-Box: Lagrangian particle tracking at high particle image densities. Experiments in fluids 57(5): 70.

Neeteson, N. J., & Rival, D. E. (2015) Pressure-field extraction on unstructured flow data using a Voronoi tessellation-based networking algorithm: a proof-of-principle study. Experiments in Fluids 56(2): 44.

Schneiders, J. F., & Scarano, F. (2016) Dense velocity reconstruction from tomographic PTV with material derivatives. Experiments in fluids 57(9): 139.

Gesemann, S. (2015) From particle tracks to velocity and acceleration fields using B-splines and penalties. arXiv preprint arXiv:1510.09034.

Wunsch, C. (1996) The ocean circulation inverse problem. Cambridge University Press.

Wang, J., Zhang, C., & Katz, J. (2019) GPU-based, parallel-line, omni-directional integration of measured pressure gradient field to obtain the 3D pressure distribution. Experiments in Fluids 60(4): 58.

Shadden, S.C., Lekien, F., & Marsden, J.E. (2005) Definition and properties of Lagrangian coherent structures from finite-time Lyapunov exponents in two-dimensional aperiodic flows. Physica D 212 (3–4): 271–304

J. Graham, K. Kanov, X.I.A. Yang, M.K. Lee, N. Malaya, C.C. Lalescu, R. Burns, G. Eyink, A. Szalay, R.D. Moser. and C. Meneveau (2016) A Web Services-accessible database of turbulent channel flow and its use for testing a new integral wall model for LES. Journal of Turbulence 17(2): 181-215.

Agarwal, K., Ram, O., & Katz, J. (2018) Cavitating structures at inception in turbulent shear flow. Proceedings for 10th International Symposium on Cavitation.